

# Biomimetic vascularized adipose-derived mesenchymal stem cells bone-periosteum graft enhances angiogenesis and osteogenesis in a male rabbit spine fusion model

Cite this article:

*Bone Joint Res* 2023;12(12):722–733.

DOI: 10.1302/2046-3758.1212.BJR-2023-0013.R1

Correspondence should be sent to Tsai-Sheng Fu [fts111@adm.cgmh.org.tw](mailto:fts111@adm.cgmh.org.tw)

T-S. Fu,<sup>1</sup> W-C. Chen,<sup>2</sup> Y-C. Wang,<sup>1</sup> C-W. Chang,<sup>1</sup> T. Lin,<sup>1</sup> C-B. Wong<sup>1</sup>

<sup>1</sup>Department of Orthopaedic Surgery, Chang Gung Memorial Hospital, School of Medicine, Chang Gung University, Taoyuan, Taiwan

<sup>2</sup>Graduate School of Biotechnology and Bioengineering, Yuan Ze University, Taoyuan, Taiwan

## Aims

Several artificial bone grafts have been developed but fail to achieve anticipated osteogenesis due to their insufficient neovascularization capacity and periosteum support. This study aimed to develop a vascularized bone-periosteum construct (VBPC) to provide better angiogenesis and osteogenesis for bone regeneration.

## Methods

A total of 24 male New Zealand white rabbits were divided into four groups according to the experimental materials. Allogenic adipose-derived mesenchymal stem cells (AMSCs) were cultured and seeded evenly in the collagen/chitosan sheet to form cell sheet as periosteum. Simultaneously, allogenic AMSCs were seeded onto alginate beads and were cultured to differentiate to endothelial-like cells to form vascularized bone construct (VBC). The cell sheet was wrapped onto VBC to create a vascularized bone-periosteum construct (VBPC). Four different experimental materials – acellular construct, VBC, non-vascularized bone-periosteum construct, and VBPC – were then implanted in bilateral L4-L5 intertransverse space. At 12 weeks post-surgery, the bone-forming capacities were determined by CT, biomechanical testing, histology, and immunohistochemistry staining analyses.

## Results

At 12 weeks, the VBPC group significantly increased new bone formation volume compared with the other groups. Biomechanical testing demonstrated higher torque strength in the VBPC group. Notably, the haematoxylin and eosin, Masson's trichrome, and immunohistochemistry-stained histological results revealed that VBPC promoted neovascularization and new bone formation in the spine fusion areas.

## Conclusion

The tissue-engineered VBPC showed great capability in promoting angiogenesis and osteogenesis in vivo. It may provide a novel approach to create a superior blood supply and nutritional environment to overcome the deficits of current artificial bone graft substitutes.

## Article focus

- Current artificial bone grafts still fail to achieve anticipated osteogenesis due to

their insufficient neovascularization capacity and periosteum support.

- Recently, adipose-derived mesenchymal stem cells have been used to fabricate tissue-engineered graft for bone healing.
- This study aimed to develop a vascularized bone-periosteum construct (VBPC) to provide better angiogenesis and osteogenesis for bone regeneration.

### Key messages

- The radiological results, biomechanical testing, and histological analysis showed VBPC has great capability in promoting angiogenesis and osteogenesis *in vivo*.
- It may provide a novel approach to create a superior blood supply and nutritional environment to overcome the deficits of insufficient vascularization capacity of current artificial bone graft substitutes.

### Strengths and limitations

- We used a standard animal bony fusion model and *in vitro* and *in vivo* comparative results.
- Current issues such as the detailed mechanism of cytokine secretion, triggered by cell-cell or cell-scaffold interactions, have yet to be clarified.
- The tissue-engineered vascularized bone-periosteum construct showed great capability in promoting angiogenesis and osteogenesis *in vitro* and *in vivo*.
- Only single-sex male animals were included in the study, and the results might therefore only be applicable to this sex.

### Introduction

With an increasingly ageing population, degenerative spinal disorders such as spondylolisthesis with spinal stenosis and osteoporotic vertebral fractures are becoming more common.<sup>1</sup> Spinal fusion surgery is increasingly performed. Using autologous bone graft is the gold standard for spinal fusion surgery owing to several critical factors: 1) a bony scaffold, 2) rich in growth factors in extracellular matrix, and 3) sufficient osteoprogenitor cells from bone marrow.<sup>2</sup> However, autologous bone graft has its own disadvantages, including donor-side morbidity and increased operating time, which has led to the development of alternative graft materials.<sup>3</sup> In addition, current synthetic bone grafts have failed to achieve anticipated fusion rates due to their insufficient vascularization capacity for new bone formation.<sup>4</sup>

Recently, mesenchymal stem cells (MSCs) from bone marrow have been used to fabricate tissue-engineered graft for bone healing.<sup>5,6</sup> However, the insufficient number of cells from bone marrow reduces their potential for clinical use. Adipose-derived mesenchymal stem cells (AMSCs) demonstrate the potential for clinical use owing to large numbers of cells.<sup>7</sup> The AMSCs can proliferate rapidly and maintain their differential potential, such as osteogenesis and angiogenesis cells, which are a good source of stem cells for bone tissue engineering.<sup>7</sup> Moreover, AMSCs secrete growth factors such as fibroblast growth factor-2 (FGF-2) and vascular endothelial growth factor (VEGF), which can stimulate the formation of new blood vessels and are extremely important for bone formation.<sup>8</sup>

From the structural perspective, the cortical bone is covered by a periosteum on its outer surface. The periosteum plays a crucial role in bone development and fracture healing.

Reports have demonstrated that periosteum not only provides skeletal stem/progenitor cells for fracture healing, but also affects cell cytoskeletal reorganization.<sup>9-11</sup> For bony tissue engineering, a biodegradable 3D scaffold is critical as a matrix for cellular adhesion, growth, differentiation, and proliferation to produce bone without eliciting inflammatory reactions. The matrix of native bone largely comprises type I collagen, which is extensively used in bone tissue engineering owing to its excellent osteoconductivity for cell proliferation and osteogenic differentiation.<sup>5-7</sup> Currently, cell sheet engineering using MSC-based preparation techniques for regenerative medicine has revealed great potential in bone healing.<sup>12-14</sup> Thus, tissue engineering approach using a periosteum-mimetic cell sheet to wrap a structural cell-impregnated scaffold might create a biomimetic bone-periosteum construct as native bone theoretically.

Chitosan (D-glucosamine linked to N-acetyl D-glucosamine by  $\beta$ -1,4-glycosidic bond), produced commercially via the deacetylation of chitin, is the main structural component of the crustacean exoskeleton and is used as a film, fibre, and porous scaffold.<sup>15,16</sup> Alginate is a natural anionic biopolymer and has antioxidant and anti-inflammatory properties for a wide variety of applications, such as wound dressing materials, 3D culture, cell and protein delivery, and cardiac regeneration.<sup>17-19</sup> A combination of chitosan and alginate may produce an ideal biocompatible and biodegradable 3D framework as a cell carrier scaffold. Based on the aforementioned reasons, we aimed to create a vascularized bone-periosteum construct (VBPC) by using an engineered biomimetic periosteum to wrap around the alginate beads seeded with epithelial-differentiated AMSCs. In this study, we hypothesized that the novel biomimetic VBPC may improve neovascularization and bone regeneration using a male New Zealand white rabbit spine fusion model *in vivo*.

### Methods

#### Ethical treatment of experimental animals

In total, 26 20-week-old adult male New Zealand white rabbits weighing 3.5 to 4 kg were used in the study. All experiments were performed in line with guidance for the care and use of laboratory animals. Animal welfare and the 3Rs (replacement, refinement, and reduction) were taken into serious consideration to guide the use of animals in this research. Approval was obtained from the Institutional Animal Care and Use Committee (IACUC) at Chang Gung Memorial Hospital (permit number: 2015121201) before the study. All the experiments were approved and supervised by the veterinary staff. Only male New Zealand white rabbits were used in the study due to lower interference of bony metabolism by genetic and hormonal factors.<sup>20,21</sup> The animals were kept in an adequately sized wire-topped plastic cage in an accredited animal facility in a controlled environment (temperature: 22°C  $\pm$  2°C, humidity: 55%  $\pm$  5%, ventilation air volume exchanged 20 times per hour, alternating 12-hour light and dark cycles). They were kept in pairs during the *in vivo* animal experiments. They were allowed free access to water and standard laboratory rodent nutrition (200 g Laboratory Rabbit Diet 5326 per day (LabDiet, USA)). Animal behaviour, appearance, movement, body weight, and wound status were closely observed and recorded with scores in a pre-defined form throughout the study period to define humane endpoints.

### Preparation of allogenic rabbit AMSCs

Two 20-week-old male New Zealand white rabbits were used for allogenic AMSC culturing. Under anaesthesia with an intramuscular injection of Zoletil (10 mg/kg weight of each rabbit) (Virbac Laboratories, France), about 3 to 4 g subcutaneous adipose tissue was collected from the neck and interscapular areas of each animal, and the operative wound was sutured with absorbable sutures. The collected adipose tissue was immersed and washed twice in phosphate-buffered saline (PBS) to clean blood clots and contaminated debris from the tissues. These were then cut into small pieces and placed in a 0.075% collagenase type I solution for 60 minutes at 37°C. The collagenase activity was neutralized with 10% fetal bovine serum (FBS) (Hyclone, USA) in low-glucose Dulbecco's Modified Eagle Medium (DMEM) (Thermo Fisher Scientific) and centrifuged at 1,200 rpm for ten minutes. The supernatant was aspirated and dissolved with PBS. Filter excess tissue with 100 µm nylon mesh. The filtrate was centrifuged at 1,200 rpm for ten minutes and the supernatant was removed. The cells were reconstituted with 20% FBS, 100 U/ml penicillin-streptomycin (Hyclone) in low-glucose DMEM, and cultured at 37°C in 5% CO<sub>2</sub> incubator.

### Flow cytometric analysis of AMSCs

After 14-day cultivation, the third-generation (P3) AMSCs were harvested using 0.25% trypsin/EDTA. A 100 µl cell suspension with a cell density of  $5 \times 10^5$ /ml was transferred into an Eppendorf tube and then incubated with specific fluorescein isothiocyanate (FITC) conjugated monoclonal antibodies, including CD9 (1:200, AbDSerotec, UK), CD29 (1:200, Sigma-Aldrich), CD44 (1:200, AbDSerotec), CD73 (1:200, Thermo Fisher Scientific), CD90 (1:200, BioLegend, UK), CD105 (1:200, Biorbyt, UK), CD45 (1:200, Thermo Fisher Scientific), and CD34 (1:200, GeneTex, USA) for 20 minutes at 4°C. Then, the stained samples were assessed by a flow cytometer (Beckman Coulter, USA) and analyzed by FlowJo software (Becton Dickinson, USA). CD9, CD29, CD44, CD73, CD90, and CD105 are commonly used as markers for various types of stem cells. CD34 and CD45 serve as cell markers for haematopoietic cells.

### Preparation of endothelial-differentiated AMSC-impregnated alginate beads (VBC)

Next, 200 mg of sodium alginate (SA) (Merck, Germany) was dissolved in 10 ml of PBS, resulting in 2% SA solution. The SA solution was heated on a hot plate and stirred thoroughly. The homogeneous SA solution was sterilized using a 0.22 µm filter. Then 10.2 ml of 1 M CaCl<sub>2</sub> stock solution was added to 89.8 ml of double-distilled water in a 100 ml volumetric flask, resulting in 102 mM CaCl<sub>2</sub> solution. The CaCl<sub>2</sub> solution was sterilized using a 0.22 µm filter. The AMSCs ( $5 \times 10^5$  cells/ml) were suspended in SA solution in a 10 ml conical tube. The mixture of AMSCs-SA was dripped into 1 ml of pre-warmed CaCl<sub>2</sub> solution. After incubation at 37°C for five minutes, CaCl<sub>2</sub> solution was discarded, and the beads were cultured in a 24-well plate with Endothelial Cell Media 2 (PromoCell, Germany).

The success of endothelial cell differentiation was confirmed by real-time polymerase chain reaction (PCR) and immunofluorescence staining analysis. For real-time PCR analysis, the samples were retrieved at three, seven, and 14 days. The total cellular RNA of the cells was extracted

with RNeasy Mini Kit (Qiagen, Germany) and reverse-transcribed into complementary DNA (cDNA) using M-MLV Reverse Transcriptase (Promega, USA). EZtime Real-Time PCR Premix (Yeastern, Taiwan) real-time PCR was used to amplify and simultaneously quantify targeted genes on oryctolagus cuniculus CD31 (Forward: TAAAATCGCCGAGAGTGGG; Reverse: AGTTCCATTTGATTGGCAGCTC) and Von Willebrand Factor (vWF) (Forward: CCGGCGATGTGTGGACC; Reverse: CCATGCACATACAGGGACAA). Each Q-PCR was performed in triplicate for PCR yield validation. Data were analyzed by the  $2^{-\Delta\Delta C_t}$  methods, with normalization by the threshold cycle of the housekeeping gene glyceraldehyde 3-phosphate dehydrogenase (GAPDH) (Forward: GGCAAAGTGGATGTTGTCGC; Reverse: TTCCCGTTCAGCCTTGAC). For immunohistochemistry (IHC) staining analysis, the samples were dehydrated and embedded with paraffin after 14 days of induction. These blocks were sectioned with the microtome at 2 µm thickness. Sections were stained with haematoxylin and eosin (H&E). For antigen retrieval, the specimens were deparaffinized and treated with 0.01 M citrate buffer (Sigma-Aldrich), pH 6.0, in a pressure cooker for one minute. For blocking of endogenous peroxidase, sections were incubated in 3% H<sub>2</sub>O<sub>2</sub> for ten minutes. The antibody against platelet endothelial cell adhesion molecule-1 (PECAM-1, CD31) (Bioss, USA) and vWF (Bioss) was used at 4°C overnight. Then, specimens were incubated in secondary antibody conjugated with Alexa Fluor 488 (Abcam, UK) for 30 minutes. Hoechst 33,342 (Thermo Fisher Scientific) was used for counterstaining.

### Preparation of engineered periosteum-mimetic cell sheet with scanning electron microscopy and fluorescence staining analysis

Overall, 1% of chitosan solution (Merck) and rat tail collagen type I solution (Sigma-Aldrich) were prepared using 1% of acetic acid, and an equal volume of each was mixed uniformly; 800 µl of the mixture was injected into a mould (length: 8.5 cm, width: 3 cm, and height: 0.1 cm). The collagen/chitosan membranes were obtained after the lyophilization process. The collagen/chitosan membranes were then washed three times at 10 cm of culture dishes. To make the periosteum-mimetic cell sheet (AMSCs seeded collagen/chitosan membrane),  $5 \times 10^5$  AMSCs were seeded in the collagen/chitosan membrane evenly at 37°C and cultivated with medium composed of low-glucose DMEM medium containing 10% of FBS and 1% of Antibiotic-Antimycotic Solution (Sigma-Aldrich) for seven days in a 5% CO<sub>2</sub> incubator. The specimens were dehydrated through a graded series of ethanol solutions, beginning with a 50% solution and progressing through 70%, 95%, and 100% solutions. The specimens were dried in a HCP-2 critical-point dryer (Hitachi, Japan) and were sputter-coated using an IB.3 ion coater (EiKo, Japan). Finally, the samples were visualized using a field emission scanning electron microscope (SEM) (Hitachi S-5000) to determine the matrix formation of AMSCs on collagen/chitosan membrane at seven days.

Fluorescence staining was used to observe the distribution of AMSCs in collagen/chitosan membrane. After a seven-day induction period, the samples were dehydrated and embedded in paraffin. Subsequently, the blocks were sectioned using a microtome to a thickness of 2 µm. The sections were then deparaffinized and treated with 0.01 M

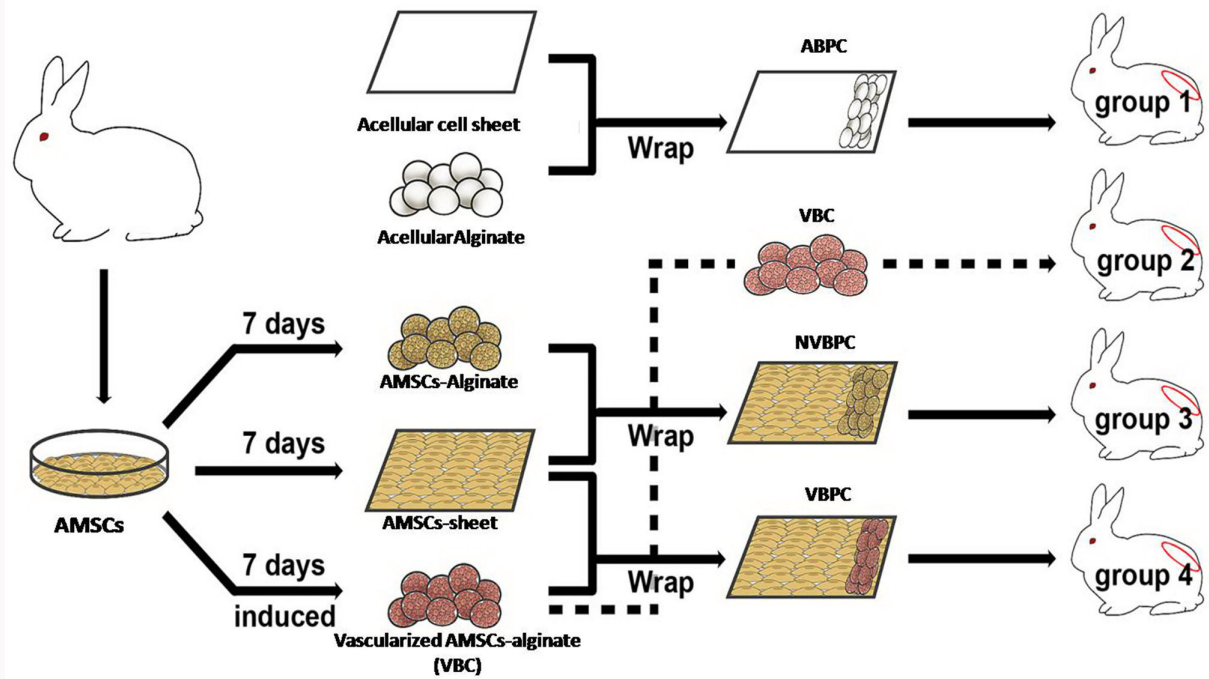


**Fig. 1**

Schematic diagram of the experimental designs and bone graft materials of a rabbit posterolateral spinal fusion model. ABPC, acellular bone construct wrapped with cell sheet ( $n = 6$ ) as a control group; AMSCs, adipose-derived mesenchymal stem cells; NVBPC, non-vascularized bone-periosteum construct; VBC, vascularized bone construct; VBPC, vascularized bone-periosteum construct.

citrate buffer (Sigma-Aldrich), pH 6.0, in a pressure cooker for one minute. To block the activity of endogenous peroxidase, the sections were incubated in 3%  $H_2O_2$  for ten minutes. Next, the specimens were incubated with actin monoclonal antibody conjugated with FITC (Thermo Fisher Scientific) for 30 minutes. Hoechst 33,342 (Thermo Fisher Scientific) was used for counterstaining. The samples were visualized using Nikon Eclipse Ti0 Microscope (Nikon, Japan).

#### Preparation of biomimetic VBPC

The alginate beads served as a bone construct (BC) scaffold. The endothelial-differentiated AMSC-impregnated alginate beads were first washed in a saline buffer, and then wrapped with periosteum-mimetic cell sheet to form biomimetic VBPC for further in vivo animal experiment.

#### In vivo animal experiment

In total, 24 male New Zealand white rabbits were randomly divided into four groups according to the four experimental materials. A surgical assistant (see Acknowledgements) prepared all experimental materials in an unlabelled manner, and the surgeon (YCW, TSF) remained blinded to the treatment throughout the entire experiment until the study conclusion. Figure 1 provides the schematic diagram of the experimental design and groups. Group 1: acellular BC wrapped with cell sheet (ABPC,  $n = 6$ ); Group 2: vascularized AMSC-impregnated BC (Figure 2a) (VBC,  $n = 6$ ); Group 3: non-vascularized AMSC-impregnated BC wrapped with cell sheet (NVBPC,  $n = 6$ ); Group 4: vascularized AMSC-impregnated alginate beads wrapped with cell sheet (Figure 2b) (VBPC,  $n = 6$ ). Under anaesthesia with an intramuscular injection of Zoletil (10 mg/kgw) (Virbac Laboratories), the

animals underwent intertransverse fusion at the L4-L5 level with different bone graft materials in an aseptic manner. The bilateral L4 and L5 transverse processes were exposed and decorticated by electric burr. The bone graft material was then placed on each side between the transverse processes (Figure 2c). The fascia and skin were closed layer-by-layer with absorbable sutures. After operation, all animals received 200 mg cefamezine per day for three days. The animals were allowed unlimited activity without brace application. In order to determine whether or not the new bone formation and neovascularization were initiated during the early stage, one rabbit in each group was killed by a pentobarbital overdose at four weeks for histological examination. After 12 weeks, the other rabbits were killed for final evaluation.

#### Radiological examination and BV/TV analysis

Five rabbits in each group underwent 2 mm thin-cut CT scanning of the lumbosacral spine at 12 weeks. The bone volume (BV) was examined in a defined total volume (TV) using ImageJ software (National Institutes for Health (NIH), USA) with the BoneJ plugin (NIH). The result of bone volume-total volume ratio (BV/TV) of each group was calculated for new bone formation. A calculated cylinder (12 mm diameter, 20 mm height) was set to the region of interest (ROI), which contained the scaffold. As a first step, the grey-value CT data were converted into binaries. The rearranged image sequence was shortened up to the height of 20 mm. Then, the bone volume in this total cylinder (12 mm diameter, 20 mm height) was calculated with the BoneJ plugin. To gain information about bone growth rates into the different sectors of the scaffold, the total cylinder was subdivided. Horizontal slices of 1 mm thickness provided information about bone distribution

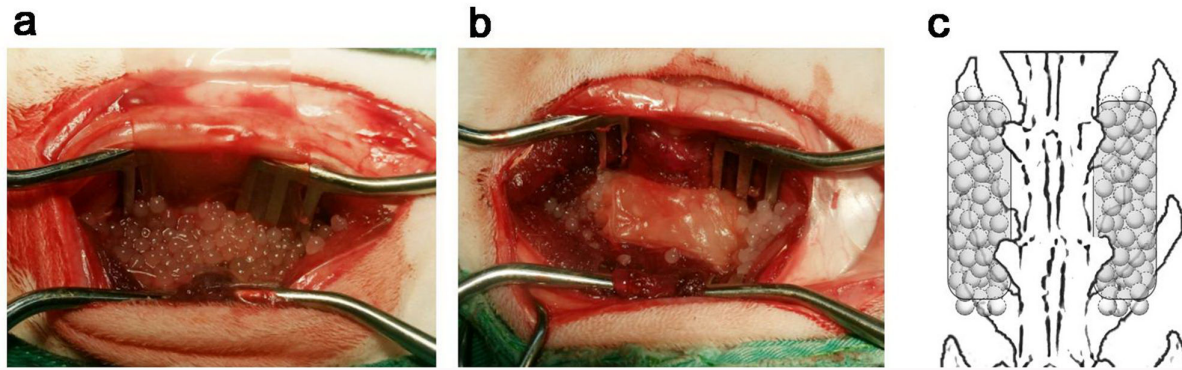


**Fig. 2**

Photographs demonstrating the appearance of the bone graft materials, and schematic of the exact anatomical location of the material implanted. a) Alginate bead materials without collagen/chitosan cell sheet wrapping. b) Alginate bead materials wrapped with collagen/chitosan cell sheet to fabricate a bone-periosteum composite implanted between L4 and L5 transverse space. c) Exact anatomical location of the material implanted in bilateral L4-L5 inter-transverse spaces.

from the surface at the cortical bone to the internal parts of the cylinder, while hollow cylinders around a central core cylinder gave insight into bone growth from the periphery to the scaffolds' centre. The L4-L5 inter-transverse fusion areas were collected for statistical analysis.

#### Biomechanical analysis

With the exception of two spine specimens that were sent for histological examination at four and 12 weeks, four rabbit spine specimens in each group were included for final biomechanical analysis. The L4-L5 fusion segment was tested for torsional biomechanical strength at 12 weeks post-surgery. The L3, L3-L4 disc, L5-L6 disc, and L6 were embedded along the longitudinal axis in cylindrically shaped epoxy blocks. The length of the L4-L5 non-embedded portion of each specimen was kept identical. The potted samples were then mounted on a Material Testing System machine (GT-7054-A1) (GOTECH Testing Machines, Taiwan) for rotational torque assessments. Each individual specimen was tested until ultimate failure in external rotation along its longitudinal axes at 1° per second. The maximum torque values were obtained from the torque-rotation angle curve. The results of maximum torque value were presented as means and standard deviations (SD).

#### Histology evaluation

The en bloc spine specimens were fixed in 10% neutral buffered formaldehyde, decalcified, dehydrated through alcohol gradients, cleared, and embedded in paraffin blocks. Tissue blocks of the intertransverse fusion areas were sectioned and stained with H&E and Masson's trichrome methods, and visualized using standard light microscopy. For immunohistochemistry staining, the slide was firstly blocked with normal goat serum for 45 minutes. Mouse anti-rabbit monoclonal primary antibodies of CD31 diluted 1:100 (Novus Biologicals, USA) were applied at 4°C for 24 hours, followed by incubation with horseradish peroxidase (HRP)-conjugated anti-mouse secondary antibody diluted in the ratio 1:250. Diaminobenzidine (Sigma-Aldrich) was used as the substrate to develop brown colour in the presence of CD31. The slides were dehydrated before being cover-slipped. The slides were dehydrated before being cover-slipped. In order to evaluate the angiogenic response, the blind count of CD31 signal

intensity was obtained within each area at a ×100 magnification microscopic field. Over ten fields were analyzed per section in a random manner, with exclusion of peripheral connective tissue. For each section, the relative signal intensity from randomly chosen fields was quantified by ImageJ. Data were expressed as signal intensity (signal pixel count divided by total image pixel count).

#### Statistical analysis

The statistical evaluation of the presented data was performed with the programs GraphPad Prism (version 5; GraphPad Software, USA) and SPSS (version 12.0; SPSS, USA). Numerical data are expressed as mean values and SDs. Statistical analysis was performed by one-way analysis of variance (ANOVA) with least significant difference post hoc testing to compare the four experimental groups with each other to determine statistical significance. Statistical significance was set at  $p < 0.05$ .

#### Results

##### Identification of rabbit AMSCs

Cell morphologies of non-differentiated AMSCs presented a spindle shape for three passages and were spread evenly on the culture dish (Figure 3a). Furthermore, the surface markers of AMSCs stained with surface antigens associated with mesenchymal stem cells (CD9, CD29, CD44, CD73, CD90, and CD105) and surface antigens associated with endothelium and haematopoiesis (CD45 and CD34) were characterized. Flow cytometry results revealed that AMSCs expressed CD9 (89.95%), CD29 (91.27%), CD44 (68.04%), CD73 (72.40%), CD90 (84.52%), and CD105 (85.61%). However, surface markers such as CD45 and CD34 associated with endothelium and haematopoiesis were not expressed (Figure 3b).

##### Endothelial differentiation of seeded AMSCs in alginate beads

The messenger RNA (mRNA) expressions of two factors, PECAM-1 (CD31) and vWF, were conducted to observe the vascularization of epithelial-differentiated AMSC-impregnated alginate beads as well as the immunofluorescence staining. The PECAM-1 mRNA expressions of endothelial-differentiated AMSCs were 2.3-, 2.6-, and 14.3-fold higher after three-day,

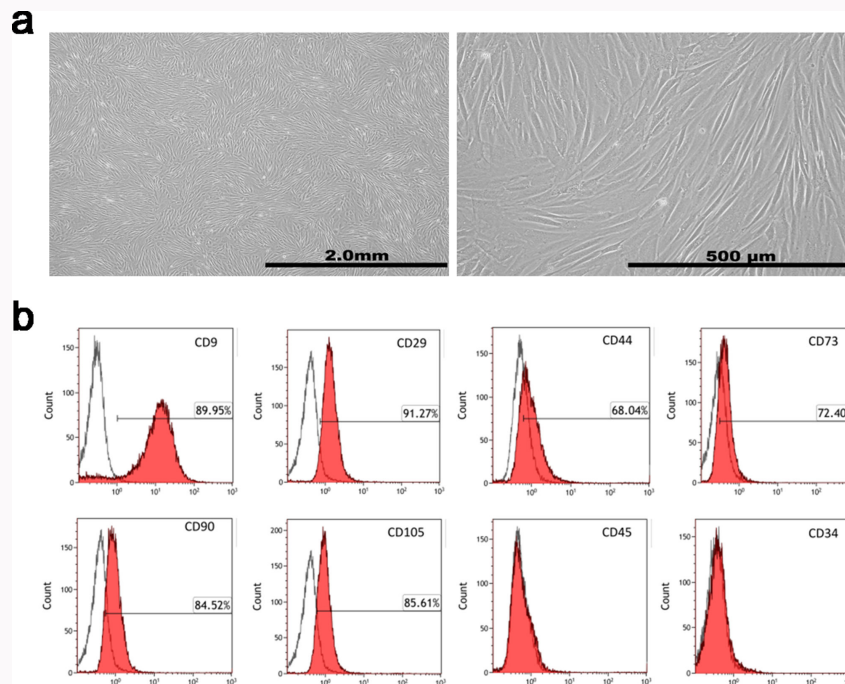


**Fig. 3**

Cell morphologies and the surface markers of adipose-derived mesenchymal stem cells (AMSCs). a) Low- ( $\times 40$ ) and high-magnification ( $\times 200$ ) microscopic observation of passage 3 non-differentiated AMSC morphologies, which show the spindle shape spread evenly on the culture dish. Scale bar: 2.0 mm and 500  $\mu\text{m}$ . b) Data from flow cytometry results showed expression of CD9 (89.95%), CD29 (91.27%), CD44 (68.04%), CD73 (72.40%), CD90 (84.52%), and CD105 (85.61%) surface antigens associated with mesenchymal stem cells. However, CD45 and CD34 surface markers associated with endothelium and haematopoiesis were not expressed.

seven-day, and 14-day cultivation compared to non-differentiated AMSCs. For vWF mRNA expression, the endothelial-differentiated AMSCs showed a 17.5-fold higher rate after 14-day cultivation compared to non-differentiated AMSCs. The mRNA expressions of PECAM-1 and vWF showed notable upregulation after endothelial differentiation; this increased sequentially by cultivation duration (Figure 4a). Notably, further time course analyses of mRNA expression showed a sharp increase of mRNA expression presented at 14-day cultivation, indicating a key timepoint for AMSCs to obtain the essential endothelial phenotype when cultured in alginate scaffolds. After 14 days' induction, the H&E-stained histology of epithelial-differentiated AMSC-impregnated alginate beads showed that the cells were evenly distributed within the porous alginate scaffold. The success of endothelial cell differentiation of AMSCs was confirmed by immunofluorescent staining of PECAM-1 and vWF (Figure 4b). In addition, self-organized tube-like structures were found. This indicated that the vascularized alginate beads had the capability of angiogenesis for further vascular network formation in vitro.

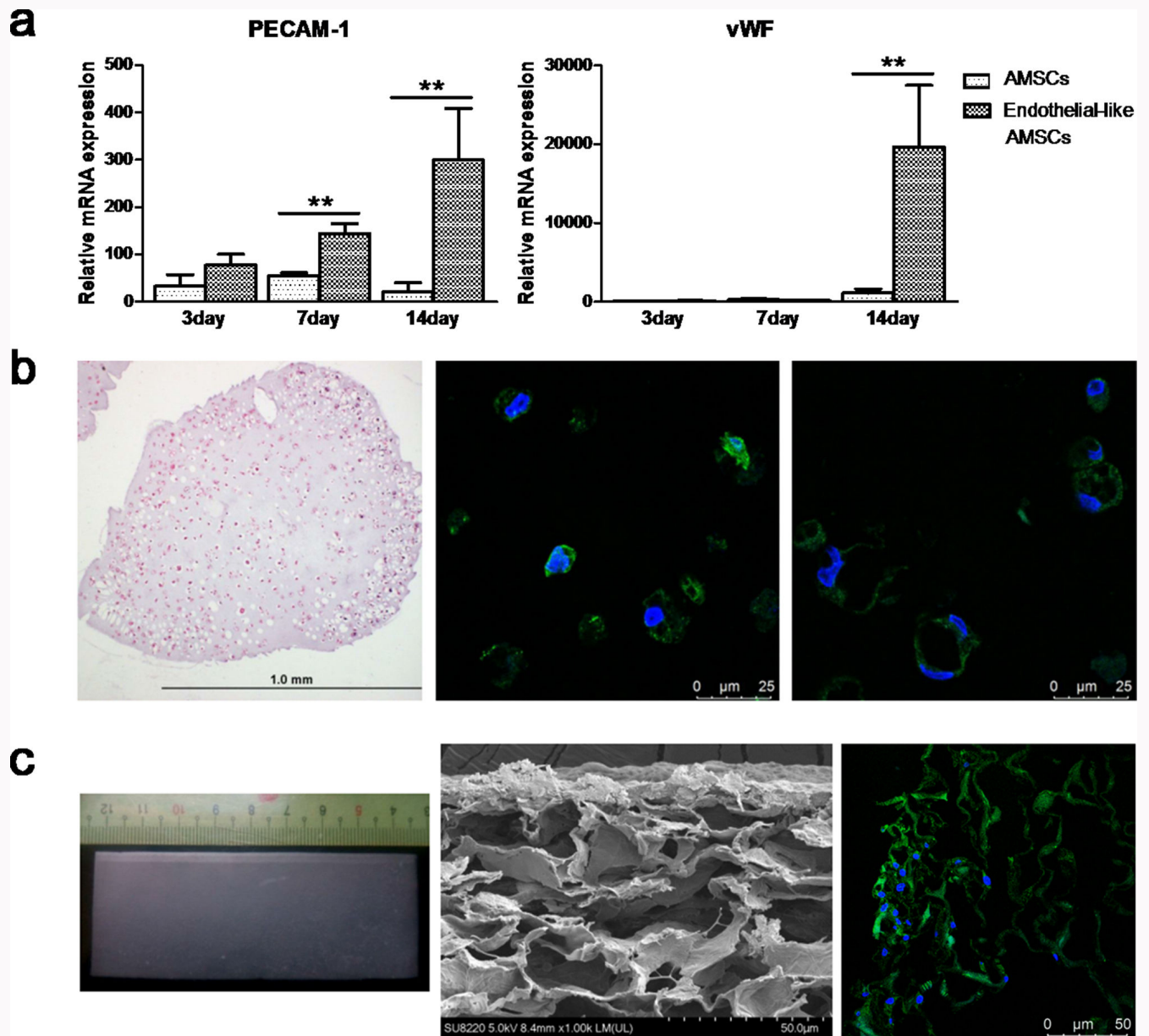
#### Analysis of periosteum-mimetic cell sheet

Figure 4c demonstrates the gross appearance and distribution of AMSCs in collagen/chitosan cell sheet. The gross view and size of the collagen/chitosan cell sheet is 8.5 cm of length, 3 cm of width, and 0.1 cm of height. The periosteum-mimetic cell sheets were obtained when AMSCs were cultivated on the collagen/chitosan cell sheet for seven days. Morphology and structures were analyzed using SEM. The morphology of the biomimetic cell sheet showed irregular lamina structures with interconnected pores. The diameter of the interconnected

pore was around 50  $\mu\text{m}$  and might have been a suitable geometry for implanted cell growth. The AMSCs grew in a flat form from the surface to interior of the cell sheet. Confocal microscopic results further showed that most AMSCs grew with a thin layer on the surface of the cell sheet and then grew into the interior area via interconnected pores. These results indicate that AMSCs could adhere to the cell sheet for further survival, proliferation, and differentiation.

#### Radiological results of in vivo animal experiment

The results of new bone formation and ossification at L4-L5 were determined by 3D CT scan reconstructive images. Figure 5a illustrated the degree of new bone formation and ossification among study groups at 12 weeks after surgery. The reconstructive coronary, axial, and sagittal cut images showed bone formation between the L4 and L5 transverse processes in all four groups, but the degree of bony ossification and continuity were different. In Group 1, reconstructive CT images showed continuous bone mass formation between L4 and L5 transverse processes. The ossified area was only located at the outer region (periosteum-mimetic cell sheets), while the inner region (acellular alginate beads) was not ossified. Unlike the other three study groups, reconstructive CT images from Group 2 showed interrupted and paper-thin bone formation between the bilateral L4 and L5 transverse processes, although high ossification was noted. The flat pattern of the new bone mass formation might be caused by the force of overlaying muscle compressing to the implanted alginate beads due to lack of cell sheet support. In Group 3, continuous bone mass formation between transverse processes with ossification at the outer region was noted,



**Fig. 4**

Differentiation of adipose-derived mesenchymal stem cells (AMSCs) into endothelial-like cells in alginate beads and AMSCs seeded in collagen/chitosan sheet. a) Platelet endothelial cell adhesion molecule-1 (PECAM-1) and vWF messenger RNA (mRNA) expression showed notable upregulation after endothelial differentiation and increased sequentially by cultivation duration, especially at day 14. b) Haematoxylin & eosin staining of alginate beads seeded with epithelial-differentiated AMSCs after 14 days' induction. The immunofluorescent staining of PECAM-1 and vWF expression confirmed the capability of angiogenesis. c) Gross appearance, scanning electron microscopy, and fluorescent confocal analyses of the cell seeded collagen/chitosan sheet.  $**p < 0.001$ .

while scattered ossification spots were observed in the centre area. In Group 4, continuous bone mass formation with evenly distributed ossification at central and outer regions between L4-L5 transverse processes was noted. The reconstructive 3D CT images revealed a continuously bridging mass between bilateral L4 and L5 transverse processes in Group 1, Group 3, and Group 4 (but not Group 2).

For quantitative evaluation of matured bone formation and ossification, the result of BV/TV ratio is shown in Figure 5b. The BV/TV ratio of each group was as follows: 0.67% for Group 1; 0.73% for Group 2; 1.21% for Group 3; and 2.28% for Group 4. Group 4 had 3.4-, 3.1-, and 1.9-fold more bone volume than Group 1 ( $p < 0.001$ ), Group 2 ( $p < 0.001$ ), and Group 3 ( $p = 0.650$ ), respectively. There was a tendency towards a higher

volume of regenerated bone in Group 4. These results indicate that VBPC facilitated the new bone formation and maturation in vivo.

#### Biomechanical strength evaluation

At 12 weeks post-surgery, L4-L5 fusion segments were secured onto the mechanical strength machine for maximal rotational torque evaluation. The mean maximal torques at failure of Group 1, Group 2, Group 3, and Group 4 were 367.17 N-mm (SD 38.59), 306.49 N-mm (SD 74.25), 331.31 N-mm (SD 45.77), and 372.69 N-mm (SD 27.97), respectively (Figure 5c). The maximal torque mean value for Group 4 was higher than for the other groups, but this was not statistically significant ( $p = 0.085$ ). Of note, the maximal torque was significantly lower for Group 2 than for the

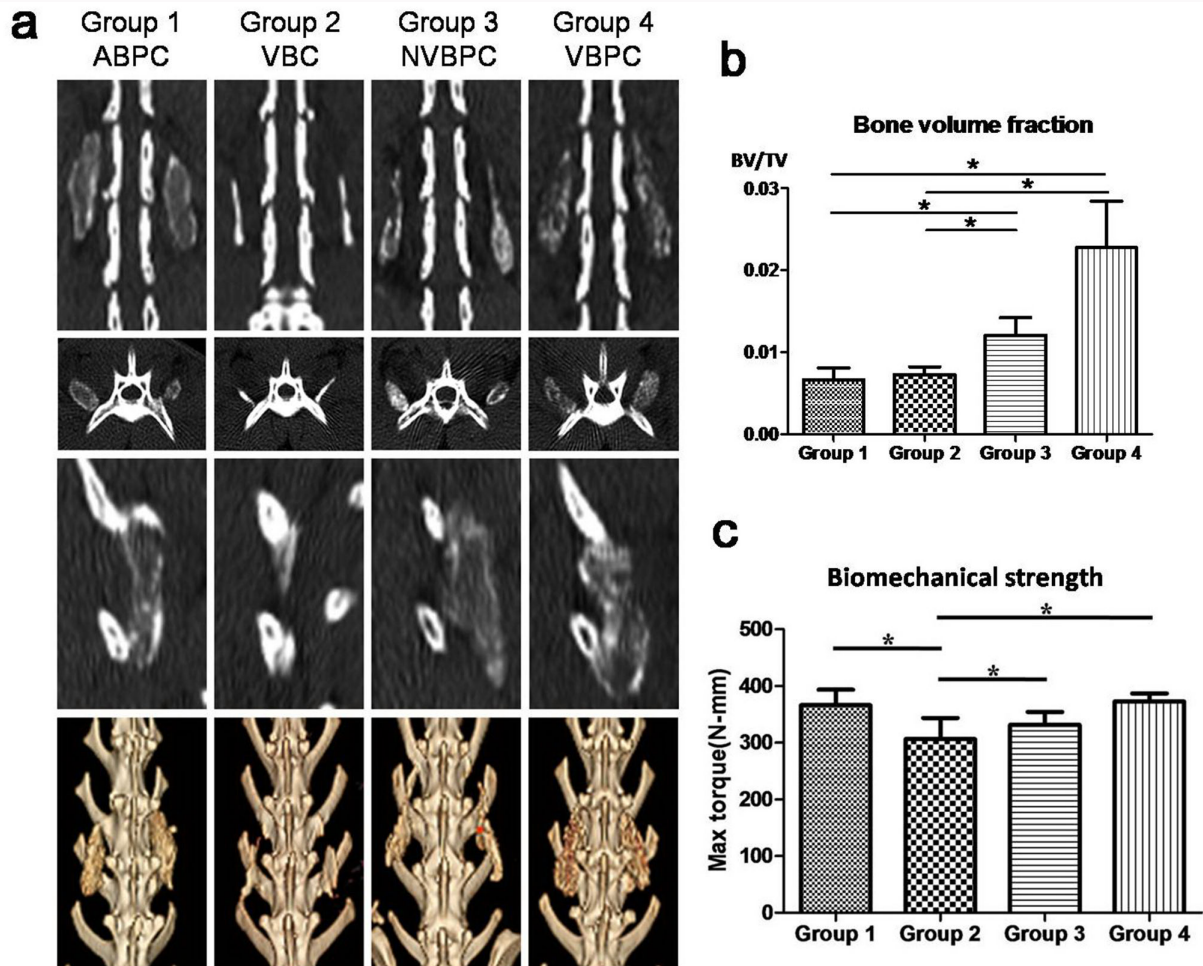


**Fig. 5**

The results of new bone formation, ossification, and biomechanical strength at 12 weeks after surgery. a) The coronal, axial, sagittal, and 3D reconstructive CT images of study groups. b) The volumetric analyses of matured bone formation; the results showed that Group 4 had a tendency towards a higher volume of regenerated bone. c) The biomechanical strength analysis showed that the maximal torque was significantly lower for Group 2 than for the other three study groups. ABPC; BV/TV, bone volume/total volume; NVBPC, non-vascularized bone-periosteum construct; VBC, vascularized bone construct; VBPC, vascularized bone-periosteum construct. \* $p < 0.05$ .

other three study groups, suggesting that the cell sheet likely played a critical role for mechanical support of alginate beads. Additionally, the maximal torque for Group 4 was marginally higher than for Group 3 ( $p = 0.055$ ), suggesting that superior bone formation and ossification were likely due to the capacity for neovascularization of VBPC graft.

### Histology evaluation

Histological analyses for healing processes and new bone formation for the four study groups were performed with consecutive sections by routine H&E and Masson's trichrome staining at four and 12 weeks (Figure 6). Histological sections at four weeks were examined to determine whether or not bone and capillary formation was initiated during the early stage. Overview of the healing processes and the results of new bone formation were evaluated at the 12-week end point. No new bone or microcapillary-like structure formation was observed in all four groups at four weeks. There was no evidence of inflammatory response to the artificial grafts in any specimens since no lymphocytic cells were detected. Notably, except Group 1, obvious cellular micropores within the alginate beads were found in the other three cell-seeded

study groups, which indicates that the impregnated cells survived and grew within the alginate beads during the early stage. After 12 weeks of survival, the alginate beads had degraded into tiny remnants and scattered within the engineered composites in all groups. There were persistent cellular micropores within the alginate remnants in Group 2 and Group 4. Self-organized tube-like structures could be observed within and between the vascularized alginate remnants, indicative of new microvascular formation via angiogenesis by the impregnated endothelial-differentiated AMSCs. On the contrary, no pores or cells could be observed within the alginate remnants for Group 1 and Group 3. This indicates that without endothelial differentiation, AMSCs could not exist within alginate beads until the late stage for further new bone formation.

At 12 weeks, a different degree of new bone formation within the inter-transverse fusion areas was observed in all groups. Thin and scattered trabecular bone formation without bridging between alginates could be observed for Group 1. Thick and bridged connecting trabecular bone formation was visible between alginate scaffolds for Group 2 and Group 4. In Group 3 specimens, thin and scattered bone formation near

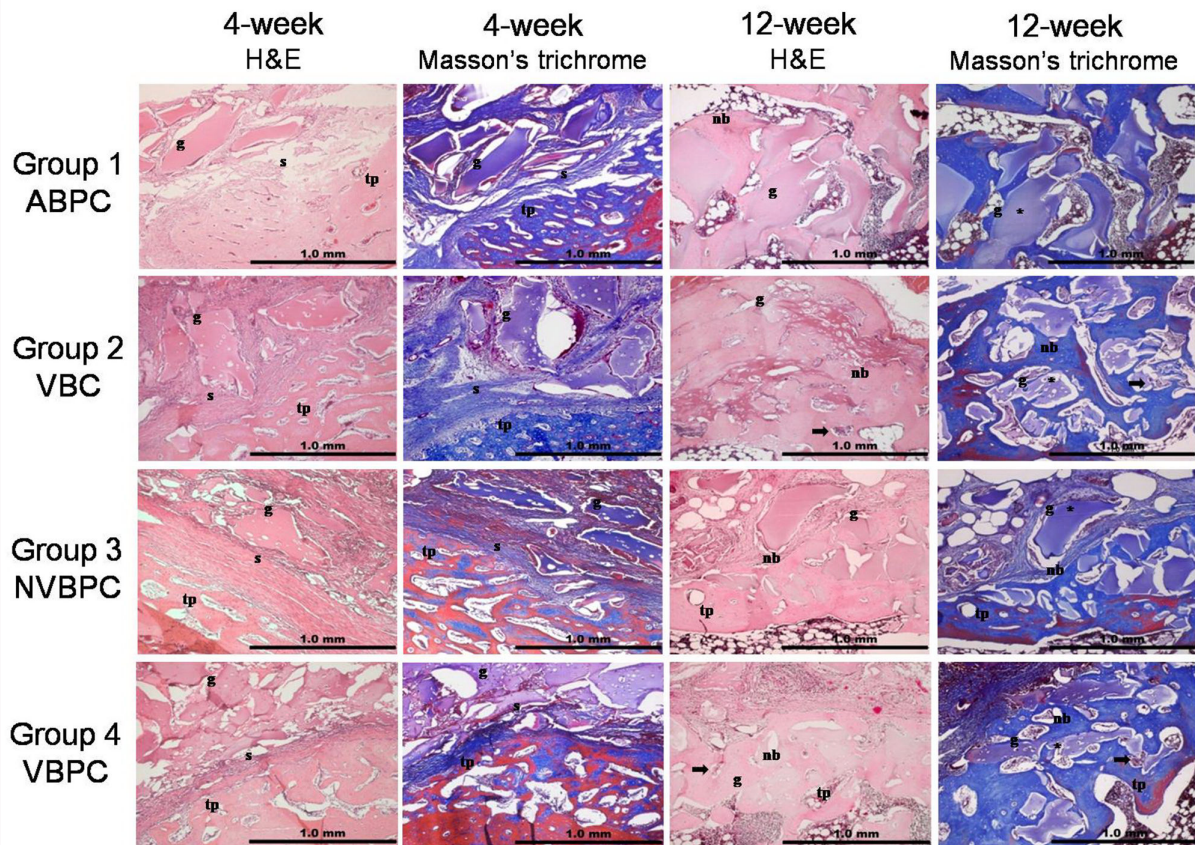


**Fig. 6**

Time course analyses of haematoxylin & eosin and Masson's trichrome stained images after implantation in vivo. Except for Group 1, cellular micropores were found within the alginate beads at the four-week early stage. Persistent cellular micropores (indicated by \*) within the alginate remnants and microvascular structures (indicated by dark arrows) were observed only in Group 2 and Group 4 after 12-week implantation. Group 2 and Group 4 showed more new trabecular bone formation between alginate scaffolds. g, residual alginate beads; nb, new bone; s, collagen/chitosan sheet; tp, transverse processes (host bone).

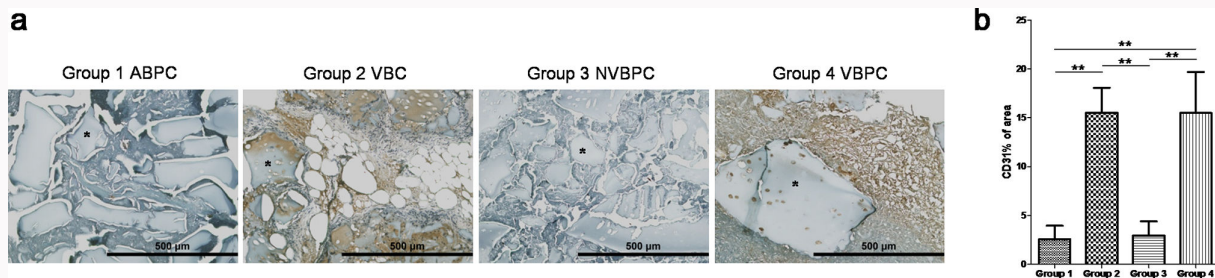


**Fig. 7**

Immunohistochemistry stain of CD31<sup>+</sup> blood vessel formation after 12-week implantation in vivo. a) Better performance of CD31<sup>+</sup> blood vessel formation (indicated by \*) appeared for Group 2 and Group 4. b) Semiquantitative analysis confirmed the image results. \*\**p* < 0.001. ABPC; NVBPC, non-vascularized bone-periosteum construct; VBC, vascularized bone construct; VBPC, vascularized bone-periosteum construct.

the transverse process and amount of fibrous tissues between alginate scaffolds could be observed.

In addition, to examine the neovascularization of bone graft in vivo, the immunohistochemistry stain of CD31<sup>+</sup> blood vessel formation in fusion area was carried out and semiquantitative analysis of the brown area was counted. The IHC results indicate that significantly better performance of CD31<sup>+</sup> blood vessel formation appeared for Group 2 and Group 4 than those for Group 1 and Group 3 (Figure 7a). Semiquantitative analysis of the CD31<sup>+</sup> IHC stained brown area confirmed that the newly formed blood vessel density for Group 2 and Group

4 was higher than that for Group 1 and Group 3 due to the endothelial differentiation of AMSCs (Figure 7b). These results indicate the capacity for angiogenesis of epithelial-differentiated AMSC-impregnated alginate beads in vivo.

### Discussion

Successful reconstruction of skeletal defects often requires bone grafting for repairing. Although the autogenous bone grafting remains the gold standard, several concerns such as limited availability, donor site morbidities, increased blood loss, and increased operating time have

prompted the search for feasible alternatives.<sup>1-4</sup> In recent years, many types of biomaterials such as bone marrow, demineralized bone matrix, collagen, and ceramics have been created for bone graft surgery to solve the defects of autogenous bone grafts.<sup>22</sup> However, the current artificial bone grafts have failed to achieve anticipated osteogenesis owing to their insufficient neovascularization capacity.<sup>4</sup> To overcome the deficit, we aimed to develop a cell-based biomimetic vascularized bone graft to create a superior neovascularization and nutritional environment for further cell growth and osteogenesis. The result was promising, and showed that incorporation of epithelial-differentiated AMSC-impregnated alginate beads and periosteum-mimetic cell sheet could create a VBPC and facilitate new bone formation as assessed in a rabbit spine fusion model. These findings implicate a relatively new approach to improve difficult bone defect management.

Recently, AMSCs have attracted attention from researchers due to the ease of obtaining these cells from small amounts of fat tissues or via liposuction, versus painful bone marrow aspirates.<sup>23</sup> Additionally, AMSCs have shown a higher rate of calcium deposition and proliferation than bone MSCs in an *ex vivo* rabbit model of calvarial defects.<sup>24</sup> Furthermore, AMSCs from subcutaneous fat tissue have demonstrated the potential to secrete multiple synergistic proangiogenic growth factors.<sup>8</sup> This evidence shows the merits of using AMSCs as a feasible cell source in bone defect repairing surgery.

Prevascularization is a prospective strategy to facilitate the vascularization of an implanted scaffold *in vivo*, demonstrating the quick integration of functional vascular networks with the host vascular system.<sup>25,26</sup> However, there is a challenge in getting effective induction of blood vessels into an engineered graft in tissue engineering. The major obstacle is to obtain an abundant source of efficient autologous endothelial cells.<sup>27</sup> Reports have shown that MSCs have the multipotent ability to differentiate into osteoblast and endothelial cells.<sup>28,29</sup> Therefore, AMSCs were induced and differentiated into endothelial-like cells by VEGF to solve the problem of the cell source of endothelial cells. Pankajakshan et al<sup>30</sup> successfully induced porcine mesenchymal stem cells to endothelial cells, which provided new options for re-endothelialization, while Liu et al<sup>31</sup> demonstrated that the co-culture rabbit MSC-derived endothelial cells improved the osteogenesis of MSCs and promoted new bone formation. Our experimental results *ex vivo* indicated that the AMSCs cultivated into alginate beads had the ability to differentiate into endothelial-like cells via the mRNA analysis of PECAM-1 and vWF. The self-organized tube-like structures within the scaffold appeared, which indicated formation of blood vessels after endothelial differentiation. Furthermore, our *in vivo* results also agreed with this phenomenon, indicating that using the VBPC could induce neovascularization around the implanted area to promote further new bone formation and ossification.

Periosteum is often used as a cell source for bone tissue engineering due to possessing a population of stem cells and osteoprogenitors. Similar to commercial bone grafts, development of engineered-membrane technology is used to replace periosteum due to obstacles in obtaining

periosteum at the traumatic site.<sup>32</sup> Several engineered-membrane technologies using collagen gel scaffold, small intestinal submucosa matrix, or thrombin-fibrinogen membrane have been reported recently.<sup>33-35</sup> These membranes are essentially composed of collagen. Their results showed that these artificial periosteums were particularly beneficial for bone regeneration. Additionally, the chitosan arises as one of the prominent materials due to its inherent biocompatibility, and antibacterial, haemostatic, and healing properties.<sup>36</sup> Kung et al<sup>37</sup> used chitosan-collagen composites to wrap around pure titanium implant surfaces. Their results showed that chitosan-collagen composites might induce *in vivo* new bone formation around pure titanium implant surfaces. Li et al<sup>38</sup> demonstrated that chitosan-collagen membranes can enhance bone regeneration in a dog dehiscence-type defect model and could be a candidate for use in guided bone regeneration. Gao et al<sup>39</sup> demonstrated that a nanofibre chitosan-collagen membrane can promote new bone regeneration effectively. These reports indicate that the combination of collagen and chitosan as a membrane can be considered a promising periosteum substitute for bone regeneration. Furthermore, the cell sheet might play an important role in preventing the alginate beads from early absorption and squeezing effects by the surrounding host tissues. As our results illustrate, the newly formed bone became flattened and discontinuous, owing to lack of cell sheet support as demonstrated by the radiological findings in Group 2. By contrast, the results of Group 3 and Group 4 showed that the cell sheet not only played an important role in new bone formation *in vivo*, but also provided the mechanical support for alginate scaffolds for further bone regeneration.

One critical point for creating a tissue engineering biomimetic bone graft is to successfully integrate the prevascularized scaffolds with the artificial periosteum into a membrane/scaffold complex. Two vital factors, cell-cell interaction and properties of scaffolds, deeply affect the success of new bone formation using an artificial periosteum-bone construct. Zhang et al<sup>40</sup> explained that tissue ingrowth might be limited because of intrinsic geometrical and structural characteristics of 3D scaffolds. The current results show that the VBPC has better neovascularization and bone formation when compared to non-vascularized grafts. We fabricated a porous cellular membrane seeded with AMSCs to mimic native periosteum. We then combined this with alginate scaffolds to produce a biomimetic periosteum-bone construct for application in the regeneration of spinal fusion surgery. The histological results *in vitro* revealed that AMSCs could grow evenly within the porous scaffolds via the interconnected micropores. Additionally, these interconnected micropores allow the circulation of nutrients and growth factors within the whole biomimetic construct, promoting a synergistic effect between the new blood vessel production, new bone formation, and mineralization.

Another critical factor that affects new bone formation *in vivo* is cell type, i.e. undifferentiated AMSCs, differentiated AMSCs (endothelial-like cells), and host cells. Reports have shown that driving stem cell differentiation toward the required lineages has been studied increasingly via co-culture of MSCs with other mature cells.<sup>5-8</sup> The cell behaviours occurred and changed either by direct or indirect cell-cell contacts between the cell types. The

mechanism by which these cells interact with each other remains unclear. The microenvironment and extracellular matrix (ECM) formed by cells may play a crucial role in osteogenic differentiation.<sup>41</sup> The ECM produced from these cells provides an appropriate microenvironment to support cell adhesion and direct cell behaviours, such as proliferation and differentiation.<sup>42,43</sup> The current results show that the numbers of newly formed blood vessels and areas of bone formation were higher in the Group 4 specimens than those of the other groups. This may be due to the endothelial differentiation of AMSCs for further angiogenesis, which indicates that more nutrients and growth factors could be obtained in the vascularized periosteum-bone groups. Although the current study does not identify the real impact factors involved in the in vivo setting for new bone formation in detail, the results demonstrate the possibility of appropriate growth factor production in the microenvironment from the interaction of undifferentiated AMSCs, differentiated AMSCs, and host cells. Currently, issues such as the detailed mechanism of cytokine secretion, triggered by cell-cell or cell-scaffold interactions, remain to be clarified. In this vein, we will continue our endeavours to elucidate the mechanisms of MSC-facilitated bone regeneration in the context of tissue engineering.

Despite the encouraging results in the current study, some limitations existed and should be addressed. First, our results could not be translated to the female sex. Only single-sex animals were included, and females were excluded due to lower interference of bony metabolism by genetic and hormonal factors.<sup>20,21</sup> Further study on both sexes is necessary to more completely characterize the efficacy of the tissue-engineered VBPC on both male and female animals. Second, the histological analysis did not analyze the active osteogenesis and osteoclastic activity among groups, nor did it specifically observe the failed area during the mechanical test of spine specimens. Further histological evaluation on the cellular activities and location of where the bone failed during the mechanical test would offer more detailed insight. Third, we only compared the bony formation for designed bone graft substitutes and did not include the standard autogenous iliac bone graft group for comparison. As the principle of institutional IACUC is to decrease the necessary number of experimental animals, and based on our previous results, we did not include the autogenous iliac bone graft group for comparison after 2009.<sup>41</sup>

In conclusion, this study demonstrated that the novel tissue engineered VBPC can promote neovascularization and bone regeneration in a male rabbit spine fusion model in vivo. The successful differentiation of AMSCs into endothelial-like cells within alginate scaffold provides the endothelial cell source for angiogenesis. The collagen/chitosan cell sheet not only acts as a periosteum, but also offers cell-impregnated alginate beads a mechanical support for further bone regeneration. This strategy demonstrates promising potential for future bone tissue engineering to regenerate bone defects, and to enhance spinal fusion success. It may provide a novel approach to create a superior blood supply and nutritional environment for osteogenesis, and to overcome the deficits of insufficient vascularization capacity of current artificial bone graft substitutes.

## Supplementary material

ARRIVE checklist to show that the animal experiments adhered to the ARRIVE guidelines.

## References

1. Gumbs AA, Bloom ND, Bitan FD, Hanan SH. Open anterior approaches for lumbar spine procedures. *Am J Surg.* 2007;194(1):98–102.
2. Vaccaro AR, Chiba K, Heller JG, et al. Bone grafting alternatives in spinal surgery. *Spine J.* 2002;2(3):206–215.
3. Fernyhough JC, Schimandle JJ, Weigel MC, Edwards CC, Levine AM. Chronic donor site pain complicating bone graft harvesting from the posterior iliac crest for spinal fusion. *Spine (Phila Pa 1976).* 1992;17(12):1474–1480.
4. Boden SD. Biology of lumbar spine fusion and use of bone graft substitutes: present, future, and next generation. *Tissue Eng.* 2000;6(4):383–399.
5. Khaled EG, Saleh M, Hindocha S, Griffin M, Khan WS. Tissue engineering for bone production- stem cells, gene therapy and scaffolds. *Open Orthop J.* 2011;5 Suppl 2(Suppl 2):289–295.
6. Cha C, Liechty WB, Khademhosseini A, Peppas NA. Designing biomaterials to direct stem cell fate. *ACS Nano.* 2012;6(11):9353–9358.
7. Zhang R, Ma J, Han J, Zhang W, Ma J. Mesenchymal stem cell related therapies for cartilage lesions and osteoarthritis. *Am J Transl Res.* 2019;11(10):6275–6289.
8. Rehman J, Traktuev D, Li J, et al. Secretion of angiogenic and antiapoptotic factors by human adipose stromal cells. *Circulation.* 2004;109(10):1292–1298.
9. Sharma A, Brand D, Fairbank J, Ye H, Lavy C, Czernuszka J. A self-organising biomimetic collagen/nano-hydroxyapatite-glycosaminoglycan scaffold for spinal fusion. *J Mater Sci.* 2017;52(21):12574–12592.
10. Vater CA, Harris ED, Siegel RC. Native cross-links in collagen fibrils induce resistance to human synovial collagenase. *Biochem J.* 1979;181(3):639–645.
11. Rasi Ghaemi S, Delalat B, Cetó X, Harding FJ, Tuke J, Voelcker NH. Synergistic influence of collagen I and BMP 2 drives osteogenic differentiation of mesenchymal stem cells: A cell microarray analysis. *Acta Biomaterialia.* 2016;34:41–52.
12. Ren L, Kang Y, Browne C, Bishop J, Yang Y. Fabrication, vascularization and osteogenic properties of a novel synthetic biomimetic induced membrane for the treatment of large bone defects. *Bone.* 2014;64:173–182.
13. Chen J, Zhang D, Li Q, et al. Effect of different cell sheet ECM microenvironment on the formation of vascular network. *Tissue Cell.* 2016;48(5):442–451.
14. Elgali I, Turri A, Xia W, et al. Guided bone regeneration using resorbable membrane and different bone substitutes: Early histological and molecular events. *Acta Biomater.* 2016;29:409–423.
15. Neves SC, Moreira Teixeira LS, Moroni L, et al. Chitosan/poly(epsilon-caprolactone) blend scaffolds for cartilage repair. *Biomaterials.* 2011;32(4):1068–1079.
16. Nettles DL, Elder SH, Gilbert JA. Potential use of chitosan as a cell scaffold material for cartilage tissue engineering. *Tissue Eng.* 2002;8(6):1009–1016.
17. Sellimi S, Younes I, Ayed HB, et al. Structural, physicochemical and antioxidant properties of sodium alginate isolated from a Tunisian brown seaweed. *Int J Biol Macromol.* 2015;72:1358–1367.
18. Nguyen V-T, Ko S-C, Oh G-W, et al. Anti-inflammatory effects of sodium alginate/gelatin porous scaffolds merged with fucoidan in murine microglial BV2 cells. *Int J Biol Macromol.* 2016;93(Pt B):1620–1632.
19. Tiwari S, Patil R, Bahadur P. Polysaccharide based scaffolds for soft tissue engineering applications. *Polymers (Basel).* 2018;11(1):1.
20. Wald C, Wu C. Of mice and women: The bias in animal models. *Science.* 2010;327(5973):1571–1572.
21. Wolf JM, Cannada L, Van Heest AE, O'Connor MI, Ladd AL. Male and female differences in musculoskeletal disease. *J Am Acad Orthop Surg.* 2015;23(6):339–347.
22. Lobb DC, DeGeorge BR, Chhabra AB. Bone graft substitutes: current concepts and future expectations. *J Hand Surg Am.* 2019;44(6):497–505.

23. **Storti G, Scioli MG, Kim BS, Orlandi A, Cervelli V.** Adipose-derived stem cells in bone tissue engineering: Useful tools with new applications. *Stem Cells Int.* 2019;2019:3673857.
24. **Lin L, Shen Q, Wei X, et al.** Comparison of osteogenic potentials of BMP4 transduced stem cells from autologous bone marrow and fat tissue in a rabbit model of calvarial defects. *Calcif Tissue Int.* 2009;85(1):55–65.
25. **Sakai Y, Nishikawa M, Evenou F, et al.** Engineering of implantable liver tissues. *Methods Mol Biol.* 2012;826:189–216.
26. **Johnson EO, Troupis T, Soucacos PN.** Tissue-engineered vascularized bone grafts: basic science and clinical relevance to trauma and reconstructive microsurgery. *Microsurgery.* 2011;31(3):176–182.
27. **Zhou L, Niu X, Liang J, et al.** Efficient differentiation of vascular endothelial cells from dermal-derived mesenchymal stem cells induced by endothelial cell lines conditioned medium. *Acta Histochem.* 2018;120(8):734–740.
28. **Böhrnsen F, Schliephake H.** Supportive angiogenic and osteogenic differentiation of mesenchymal stromal cells and endothelial cells in monolayer and co-cultures. *Int J Oral Sci.* 2016;8(4):223–230.
29. **Ren L, Ma D, Liu B, et al.** Preparation of three-dimensional vascularized MSC cell sheet constructs for tissue regeneration. *Biomed Res Int.* 2014;2014:301279.
30. **Pankajakshan D, Kansal V, Agrawal DK.** In vitro differentiation of bone marrow derived porcine mesenchymal stem cells to endothelial cells. *J Tissue Eng Regen Med.* 2013;7(11):911–920.
31. **Liu J, Liu C, Sun B, et al.** Differentiation of rabbit bone mesenchymal stem cells into endothelial cells in vitro and promotion of defective bone regeneration in vivo. *Cell Biochem Biophys.* 2014;68(3):479–487.
32. **Li N, Song J, Zhu G, et al.** Periosteum tissue engineering—a review. *Biomater Sci.* 2016;4(11):1554–1561.
33. **Gellynck K, Shah R, Deng D, et al.** Cell cytoskeletal changes effected by static compressive stress lead to changes in the contractile properties of tissue regenerative collagen membranes. *Eur Cell Mater.* 2013;25:317–325.
34. **Lindberg K, Badylak SF.** Porcine small intestinal submucosa (SIS): a bioscaffold supporting in vitro primary human epidermal cell differentiation and synthesis of basement membrane proteins. *Burns.* 2001;27(3):254–266.
35. **Göbel K, Eichler S, Wiendl H, Chavakis T, Kleinschnitz C, Meuth SG.** The coagulation factors fibrinogen, thrombin, and Factor XII in inflammatory disorders—A systematic review. *Front Immunol.* 2018;9:1731.
36. **Riaz Rajoka MS, Zhao L, Mehwish HM, Wu Y, Mahmood S.** Chitosan and its derivatives: synthesis, biotechnological applications, and future challenges. *Appl Microbiol Biotechnol.* 2019;103(4):1557–1571.
37. **Kung S, Devlin H, Fu E, Ho K-Y, Liang S-Y, Hsieh Y-D.** The osteoinductive effect of chitosan-collagen composites around pure titanium implant surfaces in rats. *J Periodontol Res.* 2011;46(1):126–133.
38. **Li X, Wang X, Zhao T, et al.** Guided bone regeneration using chitosan-collagen membranes in dog dehiscence-type defect model. *J Oral Maxillofac Surg.* 2014;72(2):304.
39. **Gao B, Li XJ, Lin M, Li YY, Dong Y.** Development of a novel absorbable nanofiber chitosan-collagen membrane by electrospinning and the preliminary study on guided bone regeneration. *Zhonghua Kou Qiang Yi Xue Za Zhi.* 2018;53(2):85–91.
40. **Zhang D, Gao P, Li Q, et al.** Engineering biomimetic periosteum with  $\beta$ -TCP scaffolds to promote bone formation in calvarial defects of rats. *Stem Cell Res Ther.* 2017;8(1):134.
41. **Fu T-S, Wang Y-C, Chen C-H, et al.** Engineered periosteum-bone biomimetic bone graft enhances posterolateral spine fusion in a rabbit model. *Spine J.* 2019;19(4):762–771.
42. **Badylak SF, Freytes DO, Gilbert TW.** Extracellular matrix as a biological scaffold material: Structure and function. *Acta Biomater.* 2009;5(1):1–13.
43. **Reilly GC, Engler AJ.** Intrinsic extracellular matrix properties regulate stem cell differentiation. *J Biomech.* 2010;43(1):55–62.

### Author information

**T-S. Fu**, MD, Orthopaedic Surgeon, Professor  
**Y-C. Wang**, MD, Orthopaedic Surgeon  
**C-W. Chang**, MD, Orthopaedic Surgeon  
**T. Lin**, MD, Orthopaedic Surgeon  
**C-B. Wong**, MD, Orthopaedic Surgeon  
 Department of Orthopaedic Surgery, Chang Gung Memorial Hospital, School of Medicine, Chang Gung University, Taoyuan, Taiwan.  
**W-C. Chen**, PhD, Associate Professor, Graduate School of Biotechnology and Bioengineering, Yuan Ze University, Taoyuan, Taiwan.

### Author contributions

**T-S. Fu**: Conceptualization, Investigation, Methodology, Resources, Writing – original draft, Writing – review & editing.  
**W-C. Chen**: Data curation, Methodology, Supervision, Validation.  
**Y-C. Wang**: Project administration, Data curation, Formal analysis.  
**C-W. Chang**: Data curation, Formal analysis, Validation.  
**T-Y. Lin**: Data curation, Supervision, Validation.  
**C-B. Wong**: Supervision, Validation, Resources.

### Funding statement

The authors disclose receipt of the following financial or material support for the research, authorship, and/or publication of this article: the study was supported by the author's institute, Chang Gung Memorial Hospital in Keelung (grant numbers CMRPG2G0201, CMRPG2I0051, and CMRPG2H0071).

### ICMJE COI statement

The study was supported by the author's institute, Chang Gung Memorial Hospital in Keelung (grant numbers CMRPG2G0201, CMRPG2I0051, and CMRPG2H0071)

### Data sharing

The data that support the findings for this study are available to other researchers from the corresponding author upon reasonable request.

### Acknowledgements

We would like to thank our research assistant Shih-Hui Chen (MSc) for her help and contribution to the experiments and animal care.

### Ethical review statement

Animal welfare and the 3Rs (replacement, refinement, and reduction) were taken into serious consideration to guide the use of animals in this research. Approval was obtained from the Institutional Animal Care and Use Committee (IACUC) at the authors' institute (permit number: 2015121201) before the study.

### Open access funding

The open access fee for this article was self-funded.

© 2023 Fu et al. This is an open-access article distributed under the terms of the Creative Commons Attribution Non-Commercial No Derivatives (CC BY-NC-ND 4.0) licence, which permits the copying and redistribution of the work only, and provided the original author and source are credited. See <https://creativecommons.org/licenses/by-nc-nd/4.0/>